



© 2022 Geological Society of America. For permission to copy, contact editing@geosociety.org

Manuscript received 20 November 2021 Revised manuscript received 15 January 2022 Manuscript accepted 26 January 2022

Published online 24 March 2022

Nanoscale trace-element zoning in pyrite framboids and implications for paleoproxy applications

Daniel D. Gregory¹, Libor Kovarik², Sandra D. Taylor², Daniel E. Perea³, Jeremy D. Owens⁴, Nicole Atienza¹ and Timothy W. Lyons⁵

- Department of Earth Sciences, University of Toronto, Toronto, Ontario M5S 3B1, Canada
- ²Physical and Computational Sciences Directorate, Pacific Northwest National Laboratory, Richland, Washington 99354, USA
- ³Earth and Biological Sciences Directorate, Environmental Molecular Sciences Laboratory, Pacific Northwest National Laboratory, Richland, Washington 99354, USA
- ⁴National High Magnetic Field Laboratory, Florida State University, Tallahassee, Florida 32306, USA
- Department of Earth and Planetary Sciences, University of California, Riverside, California 92521, USA

ABSTRACT

Pyrite framboids (spherical masses of nanoscale pyrite) are among the earliest textures of pyrite to form in sediments. It has been proposed that their trace-element (TE) contents can be used to track the TE composition of the water column in which they formed. However, it is not clear how these TEs are associated with the framboidal pyrite grains. For instance, it is important to know whether they are incorporated uniformly or are enriched in different regions of the framboid. We used high-resolution scanning transmission electron microscopy to identify chemical zoning within pyrite framboids. We found that initial, nanoscale pyrite euhedral crystals, which make up the volumetric majority of the framboids, are covered/ infilled by later pyrite that templates on the earlier pyrite. Further, this later pyrite is enriched in TEs, suggesting that many TEs are incorporated in pyrite relatively late (during early diagenesis; not in the water column). This observation suggests that although chemical analyses of pyrite framboids may provide ocean-water chemistry trends through time, the details are complex. Specifically, the TEs found in pyrite may be linked to adsorption onto organic matter, detrital material, and authigenic minerals such as Fe- and Mn-oxide phases followed by desorption in the sediments or release via dissolution and incorporation into pyrite as overgrowths on the initial nanoscale euhedral crystals that make up framboids. While the use of pyrite chemistry to understand past ocean conditions remains promising, and even diagenetic additions may not preclude the utility of pyrite for reconstructing ancient ocean conditions, care must be taken in interpretations because the end concentration may be influenced by diagenesis.

INTRODUCTION

Pyrite trace-element (TE) contents have relevance to many different aspects of the earth sciences, including past ocean chemistry (Large et al., 2014, 2019; Gregory et al., 2017), mineral deposit formation (Genna and Gaboury, 2015; Gregory et al., 2016), ore deposit source rock fertility (Sack et al., 2018), problematic building materials (Dornan et al., 2020), sequestration of environmentally detrimental metals and metalloids (Lowers et al., 2007), and the semiconductor properties of pyrite (Abraitis et al., 2004). However, the mechanism of incorporation of TEs into early formed pyrite in sedimentary settings is not well understood and is likely controlled by a combination of TE concentrations

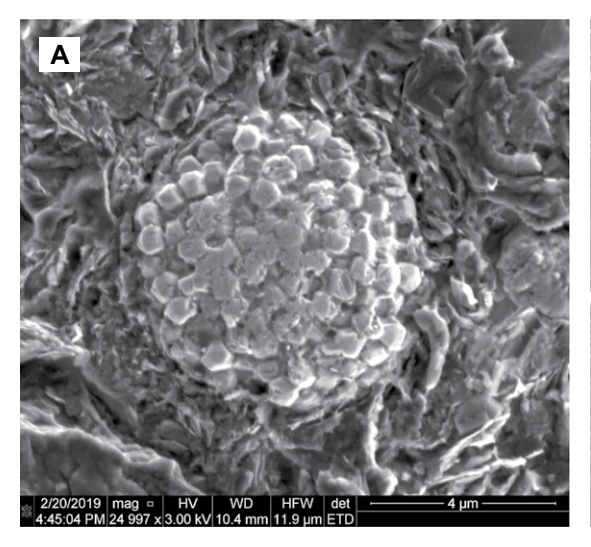
in the surrounding environment, competition between pyrite and other sediment components, and pyrite crystal chemistry (Rickard, 2021). Early formed pyrite typically forms clusters of equidimensional and equimorphic microcrystals that are spheroidal to subspheroidal (Ohfuji and Rickard, 2005) called framboids. Rickard (2012, 2021) provided a detailed discussion of how framboids form (Fig. 1A). Determining how TEs are incorporated in pyrite requires high-resolution analyses of TE distributions to track the progression of uptake and specifically the relationship between TE concentrations in the framboids and in the surrounding reservoirs at the time of formation. The most critical factors are understanding the ways in which initial

depositional waters are recorded rather than conditions present during early and later burial, and when the individual signals, when combined in a single framboid, are resolvable.

The incorporation of TEs into pyrite framboids has received significant attention in recent years and has been summarized in detail by Rickard (2021), a brief summary of which is given here. Sequential extraction analyses of bulk sediments showed that TEs tend to increase in the pyrite fraction with increasing depth in the sediments, suggesting some incorporation during diagenesis (Huerta-Diaz and Morse, 1992). Due to the inherent nonspecificity of reagents in sequential extraction analyses (Martin et al., 1987), however, these studies could not confirm quantitative and selective extraction of pyrite.

Improvement was sought by analyzing pyrite mechanically separated from sedimentary rocks (Berner et al., 2013). However, while this approach outlined probable trends, it could not provide definitive evidence for the timing or the locations of TEs in pyrite. Gregory et al. (2014) used TE variation as pyrite was ablated to identify zoning for various elements within pyrite framboids; however, the 10 µm scale of the laser spot was still too coarse to determine whether TEs were structurally held or distributed evenly in nano-inclusions. Nanoscale secondary ion mass spectrometry (NanoSIMS) has also been employed to probe the chemical makeup of pyrite framboids and specifically to identify incorporation of organic matter (Wacey et al., 2015). More recently, laser ablation-inductively coupled plasma-mass spectrometry (LA-ICP-MS) analyses of pyrite TE (Co, Ni, Cu, Mo, Ag, and Bi) contents have been shown to increase with depth in the upper 30-70 cm of sediments

CITATION: Gregory, D.D., et al., 2022, Nanoscale trace-element zoning in pyrite framboids and implications for paleoproxy applications: Geology, v. 50, p. 736-740, https://doi.org/10.1130/G49890.1



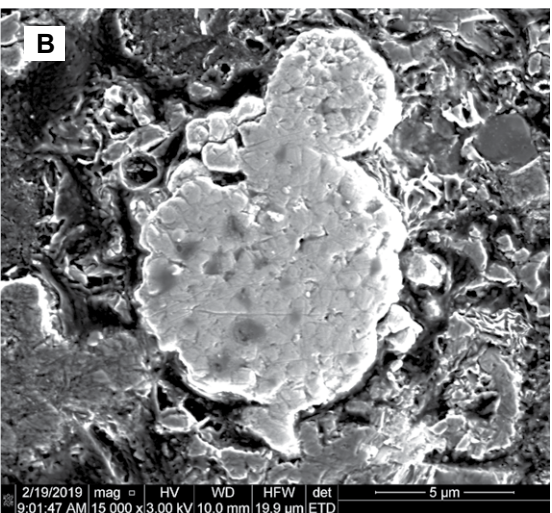


Figure 1. Scanning electron microscope (SEM) images of pyrite framboids analyzed by transmission electron microscopy (TEM) from (A) the Cariaco Basin, offshore Venezuela (recent) and (B) the Demerara Rise (Cretaceous proto-Atlantic Ocean).

deposited under euxinic conditions (in Cariaco Basin [offshore Venezuela] and the Black Sea; Gregory et al., 2022), suggesting that at least a component of pyrite TE uptake occurs within the sediments, even in areas of euxinic deposition. However, the nature of the TE enrichment was still elusive due to the size of the laser spot $(10 \ \mu m)$ used for these analyses.

To overcome these difficulties, we present nanometer-scale transmission electron microscope (TEM) TE maps of pyrite framboids deposited under euxinic conditions from two different sites at different times in Earth history, the Cariaco Basin (recent) and the Demerara Rise (Cretaceous proto—Atlantic Ocean). These analyses yielded nanometer-scale identification of TE zoning in pyrite framboids that delineates the timing of TE incorporation.

SAMPLE LOCATIONS

Samples were taken from two sediment cores to minimize the risk that the framboids had been altered by weathering or metamorphic fluids. The first sample was taken from the Cariaco Basin from Ocean Drilling Program (ODP) Site 1002 (10°42.4'N, 65°10.2'W) at a sediment depth of 365 cm. The second sample was collected from the Demerara Rise at ODP Site 1258 (9°26′N, 54°44′W) from a composite depth of 426.56 m below the seafloor. Both samples were deposited under a sulfidic (euxinic) water column (Lyons et al., 2003; Owens et al., 2016), and it is interpreted that significant pyrite was formed in the water column (Raven et al., 2019; Bryant et al., 2020). The Demerara Rise sample was taken below the sediments deposited during Ocean Anoxic Event 2. Thus, both samples represent local euxinia at times when such conditions were not globally extensive (i.e., no evidence for TE drawdown at an ocean scale).

METHODS

Samples were mounted in epoxy and polished. They were then imaged using a JEOL

JSM-6610LV scanning electron microscope (SEM) at the University of Toronto (Canada) (Fig. 1). TEM lamellar foils were created using a Helios Nanolab 600i focused ion beam SEM at the Environmental Molecular Sciences Laboratory in the Pacific Northwest National Laboratory (Washington State, USA). Scanning transmission electron microscope (STEM) analysis was performed with a probe-corrected FEI Titan 80-300 TEM operated at 300 kV. The STEM observations were performed with a probe convergence angle of 18 mrad. A high-angle annular dark-field (HAADF) detector was used for the STEM observations, with an inner detection angle three times higher than the probe convergence angle. TEM and diffraction observations were performed using a Gatan UltraScan1000 2K×2K charge-coupled device (CCD) camera. Compositional analysis was performed with energy-dispersive spectroscopy (EDS) using an Oxford X-MaxN 100TLE solid drift detector (SDD; 100 mm²). The EDS data collection and processing were performed with Oxford's AZtec software package (https://nano.oxinst .com/products/aztec/).

RESULTS

Representative framboids were chosen from both the Cariaco Basin and Demerara Rise samples (Fig. 1). The TEM images show two distinct textures associated with the framboids: (1) nonporous, euhedral crystals, and (2) more porous pyrite that coats the euhedral crystals (Figs. 2A and 3A). To determine whether these are two pyrite generations and not pyrite precursor minerals, electron diffraction analyses were performed on representative examples (see the Supplemental Material¹). This effort yielded dif-

fraction data confirming isometric crystals with lattice parameter $a=5.4\,\text{Å}$, which is consistent with pyrite. Also, compositional Fe/S ratios and lattice image spacing and symmetry are both consistent with pyrite. We thus concluded that both the euhedral, nonporous crystals and the porous overgrowths are pyrite.

It has been long known that pyrite framboids consist of euhedral crystals that are nanometers in diameter (Figs. 2 and 3). We show that a second, presumably later, generation of pyrite (the porous pyrite) formed on the edges of the early euhedral grains in both the Cariaco Basin (Fig. 2B) and Demerara Rise (Fig. 3B) samples. In the highmagnification images (Figs. 2C and 3C), the later pyrite contains several low-density regions (darker areas in the TEM), possibly indicating void space or inclusion of less dense material, such as organic matter. Importantly, the porous region seems to be thicker and better developed in the Cretaceous Demerara Rise sample, where it forms an \sim 20-nm-thick layer on the edges of the euhedral grains, compared to the relatively recent Cariaco Basin samples. We also observed that Cu and Ni are zoned in the framboids. Specifically, the noneuhedral regions of the framboids have relatively more of these TEs compared to the more euhedral crystals. Interestingly, the later pyrite overgrowths appear to have used the earlier pyrite as a template. This observation is clear in Figure 4, where high-resolution STEM imaging shows that the orientations of atoms in both pyrite generations are the same, defining a crystallographically coherent interface between the atoms of the early euhedral microcrystals (bottom) and the more porous pyrite (top).

DISCUSSION

Pyrite framboids are known to form quickly over intervals ranging from days to weeks (Rickard, 2019) and are not significantly altered through geologic time (Rickard, 2019). Due to their rapid formation, the TE content of the pyrite may faithfully reflect the environment

¹Supplemental Material. More-detailed TEM methodology. Please visit https://doi.org/10.1130 /GEOL.S.19308965 to access the supplemental material, and contact editing@geosociety.org with any questions.

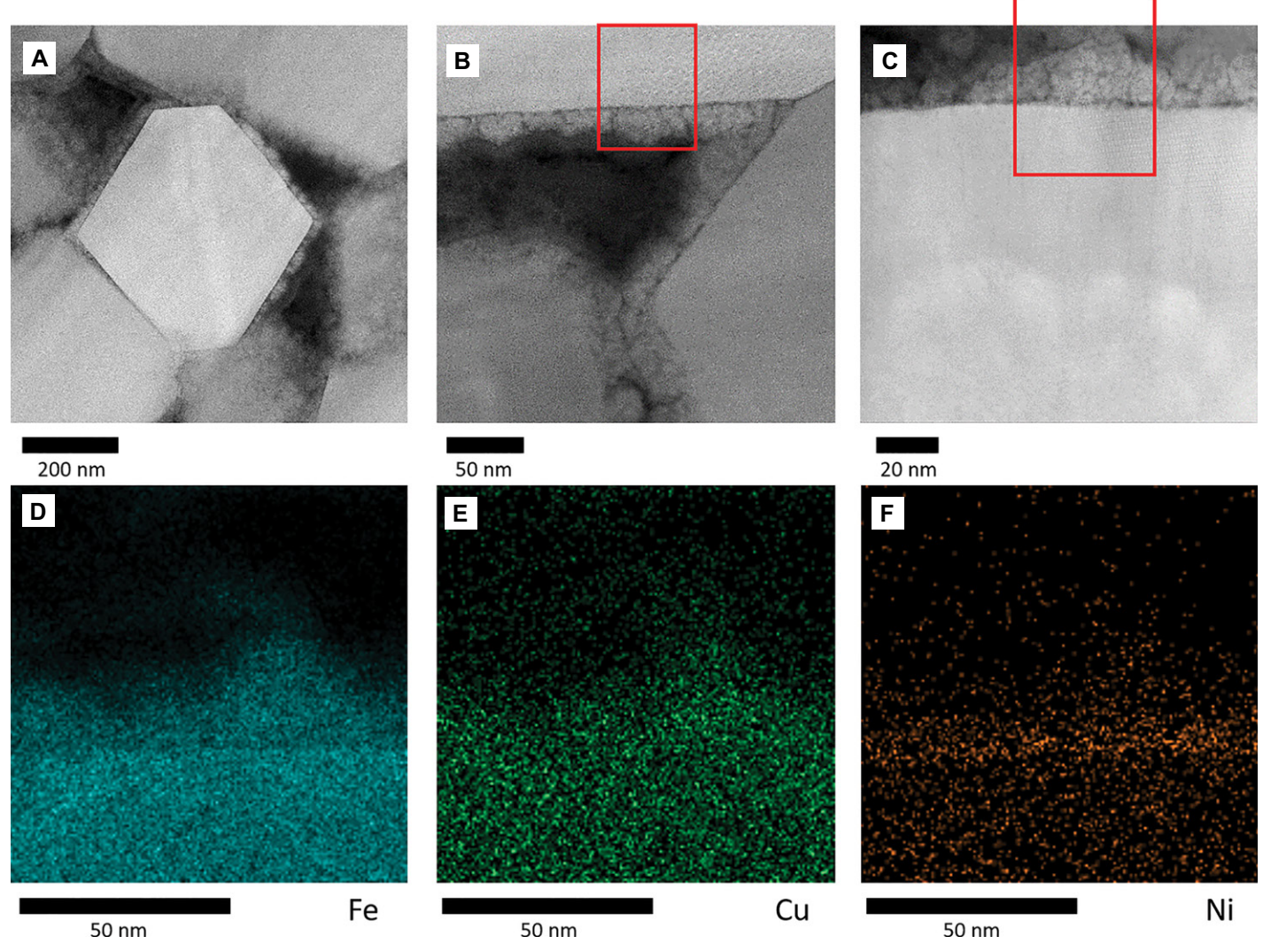


Figure 2. (A–C) Transmission electron microscope (TEM) images of pyrite framboid from Cariaco Basin, offshore Venezuela. These images show early euhedral pyrite microcrystals being overgrown by later porous pyrite. (D–F) Fe abundance (D) gives a reference point for location of pyrite in the sample for comparison with later Cu and Ni maps (E and F, respectively). Fe is lower in later pyrite, due to lower-density areas identified by TEM. Cu (E) is slightly enriched in outer pyrite, though extent of relative enrichment is unclear. Ni (F) is clearly enriched at interface between early euhedral pyrite and porous overgrowth.

of formation—particularly when formed in the water column. However, the two phases of pyrite formation associated with the framboids here suggest that formation may have extended through burial, potentially complicating the interpretation of the pyrite TE record and specifically the connections between those data and the overlying water column.

The later pyrite overgrowths in the framboids result from a combination of relative sulfur and Fe availability. This relationship can manifest in several ways. In the sites investigated here, S was likely to be the most abundant element, as these sediments were deposited under euxinic conditions. Even if the pore-water HS⁻ were depleted, later reactions linked to sulfidized organic matter (e.g., Raven et al., 2019) could lead to diagenetic pyrite formation. However, at less S-rich sites (beneath anoxic but noneuxinic or oxic water columns), S may be a limiting

element. Fe availability is likely to change with time in a given setting, varying as a result of the composition of sediments and the redox state of the overlying waters. Dissolved Fe is largely depleted during the initial, rapid nucleation of pyrite (Rickard, 2021), which results in the inner euhedral, less porous parts of the framboids in Figures 2 and 3. Any remaining Fe will either be adsorbed onto organic matter and other detrital particles or be bound to metastable minerals that break down during diagenesis. When released, this Fe will have lower concentrations than were present when the initial pyrite framboids formed and will nucleate on the earlier pyrite seed crystals, as this mechanism for pyrite formation requires a lower degree of supersaturation (Rickard, 2012). Depending on the concentration of available Fe and S, the amount of pyrite overgrown on the seed crystals will vary. This relationship is shown in the Demerara

Rise sample, which has larger, more complete overgrowths of later pyrite relative to the Cariaco Basin sample (Figs. 2 and 3) because the Demerara Rise sample had a comparatively high concentration of available Fe. Consistent with this observation, the Demerara Rise pyrite shows relatively positive δ^{34} S values ($\sim 0\%e$) (Raven et al., 2019), pointing to more comprehensive uptake of the available S.

Enrichments in the later, intergrain pyrite show that the overgrowths contain a significant proportion of the Ni and Cu in the framboid. This is consistent with LA-ICP-MS analyses that show a progressive increase in TE content (Ni, Cu, Co, Mo, Ag, and Bi) with increasing depth in the Cariaco Basin and Black Sea, tracking TE incorporation into pyrite framboids during early burial diagenesis (Gregory et al., 2022). It is also consistent with sequential leach extractions of TEs in the pyrite fraction (Huerta-Diaz

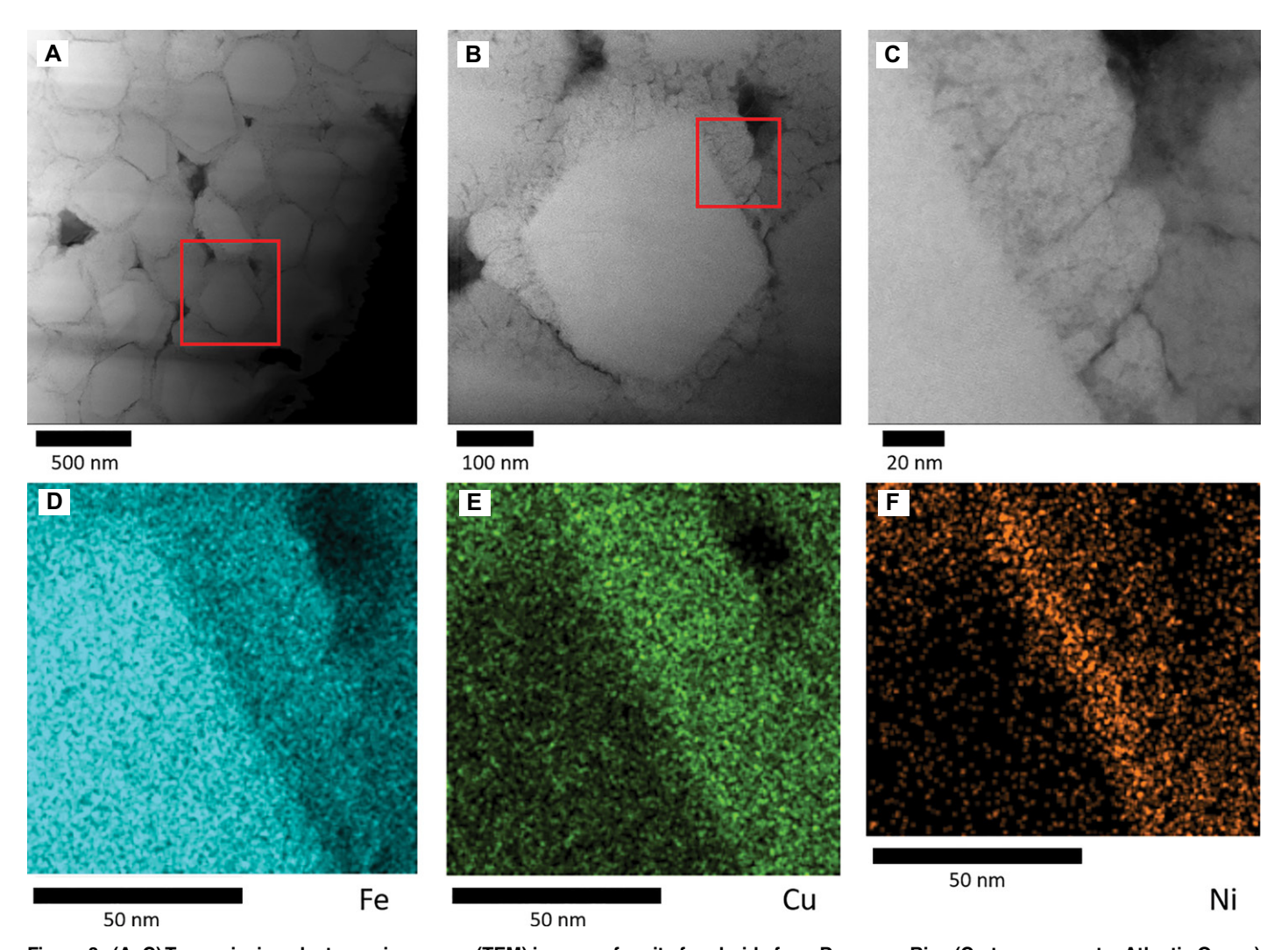


Figure 3. (A–C) Transmission electron microscope (TEM) images of pyrite framboids from Demerara Rise (Cretaceous proto–Atlantic Ocean) prior to Ocean Anoxic Event 2 (OAE2). These images show early euhedral pyrite microcrystals being overgrown by later porous pyrite. Note that later, porous pyrite is more well developed than in Cariaco Basin (offshore Venezuela) (Fig. 1). (D–F) Fe abundance (D) gives a reference point for pyrite in the sample for comparison with later Cu and Ni maps (E and F, respectively). Fe is lower in later pyrite, due to lower-density areas identified by TEM. Cu (E) is enriched in outer pyrite. Ni (F) is also enriched at interface between early euhedral pyrite and porous overgrowth.

and Morse, 1992) and LA-ICP-MS analyses of pyrite in modern estuarine sediments (Gregory et al., 2014), which both show that TEs in pyrite

increase with sediment depth. Thus, pyrite TE records can capture both conditions in the water column and TEs remobilized during diagenesis

10 nm

Figure 4. High-magnification image of a Cariaco Basin (offshore Venezuela) pyrite framboid. Alignment of atoms can be seen from the euhedral pyrite crystal continuing into later, porous pyrite. This indicates that later pyrite is templating on earlier, euhedral pyrite.

from detrital minerals, organic matter, and authigenic Fe and Mn oxides.

The observations of this study are important for reconstructions of past ocean chemistry because they tell us that diverse parameters that vary under different conditions—such as water-column redox, rates of deposition, and organic sinking flux-must be considered when assessing if and how the final stages of pyrite formation and the bulk framboid composition reflect past metal inventories in the oceans. Since the bulk pyrite framboid TE content can be affected by progressive pyrite formation over many tens of centimeters of burial in pore waters with evolving TE concentrations (Gregory et al., 2014, 2022), the ideal application of the proxy lies with pyrite that locks in its bulk TE content early in the sediments or, even better, in the water column. However, because TE uptake during early burial likely derives from weakly bound TEs adsorbed to organic matter and mineral phases that ultimately reflect the

same overarching marine environment, pyrite can reflect the composition of the overlying waters in a first-order way, whether mostly formed in the water column, the sediments, or both. This general agreement manifests in comparisons of pyrite data to whole-rock TE content through time (Large et al., 2014; Gregory et al., 2015), and the utility of the pyrite approach is elevated because TE contents can be preserved more completely during metamorphism (Large et al., 2009). Thus, despite the complications of multigenerational formation, pyrite chemistry can tell us much about broad spatiotemporal patterns of metal abundances in the coeval seawater on a variety of time scales (Large et al., 2014, 2019; Gregory et al., 2019).

CONCLUSIONS

Using TEM imaging of thin slices of pyrite framboids, we observed two distinct phases of pyrite formation in framboids, even when deposited in euxinic settings, where most pyrite is thought to form in the water column. Further, TEs can be concentrated in later generations of pyrite that are formed within the sediment in pore waters having TE contents that differ from the overlying waters. These relationships show that multiple potential factors need to be taken into account when interpreting past ocean chemistry, while also offering opportunities for tracking the past availability of TEs for microbial life in sediments. However, because metal inventories in these subsurface systems ultimately scale with metals present in the ocean, bulk pyrite—even when influenced by diagenetic overprints-can and often does capture first-order oceanic metal inventories.

ACKNOWLEDGMENTS

Analyses were performed using the Environmental Molecular Sciences Laboratory (grid.436923.9), a U.S. Department of Energy Office of Science User Facility sponsored by the Biological and Environmental Research program (proposal ID 50756 to D. Gregory and proposal ID 49860 to T. Lyons). We acknowledge a Natural Sciences and Engineering Research Council of Canada Discovery grant to D. Gregory. J. Owens acknowledges support from the National Aeronautics and Space Administration (NASA) Exobiology Program (80NSSC18K1532), and the National High Magnetic Field Laboratory (Tallahassee, Florida), supported by National Science Foundation Cooperative Agreement DMR1644779 and the State of Florida. We also thank reviewers David Rickard, Nicolas Tribovillard, Ross Large, and M.L. Dora, and editor Kathleen Benison, for comments that greatly improved the manuscript.

REFERENCES CITED

Abraitis, P., Pattrick, R., and Vaughan, D., 2004, Variations in the compositional, textural and electrical properties of natural pyrite: A review: International Journal of Mineral Processing, v. 74, p. 41–59, https://doi.org/10.1016/j.minpro.2003.09.002.

- Berner, Z. A., Puchelt, H., Nöltner, T., and Kramar, U.T.Z., 2013, Pyrite geochemistry in the Toarcian Posidonia Shale of south-west Germany: Evidence for contrasting trace-element patterns of diagenetic and syngenetic pyrites: Sedimentology, v. 60, p. 548–573, https://doi.org/10.1111/j.1365-3091.2012.01350.x.
- Bryant, R., Jones, C., Raven, M., Owens, J., and Fike, D., 2020, Shifting modes of iron sulfidization at the onset of OAE-2 drive regional shifts in pyrite δ³⁴S records: Chemical Geology, v. 553, 119808, https://doi.org/10.1016/j.chemgeo.2020.119808.
- Dornan, T., O'Sullivan, G., O'Riain, N., Stueeken, E., and Goodhue, R., 2020, The application of machine learning methods to aggregate geochemistry predicts quarry source location: An example from Ireland: Computers & Geosciences, v. 140, 104495, https://doi.org/10.1016/j.cageo.2020 104495
- Genna, D., and Gaboury, D., 2015, Deciphering the hydrothermal evolution of a VMS system by LA-ICP-MS using TEs in pyrite: An example from the Bracemac-McLeod deposits, Abitibi, Canada, and implications for exploration: Economic Geology, v. 110, p. 2087–2108, https://doi.org/10 .2113/econgeo.110.8.2087.
- Gregory, D., Meffre, S., and Large, R., 2014, Comparison of metal enrichment in pyrite framboids from a metal-enriched and metal-poor estuary: The American Mineralogist, v. 99, p. 633–644, https://doi.org/10.2138/am.2014.4545.
- Gregory, D.D., Large, R.R., Bath, A.B., Steadman, J.A., Wu, S., Danyushevsky, L., Bull, S.W., Holden, P., and Ireland, T.R., 2016, TE content of pyrite from the Kapai Slate, St. Ives Gold District, Western Australia: Economic Geology, v. 111, p. 1297–1320, https://doi.org/10.2113/econgeo 111.6.1297
- Gregory, D.D., Large, R.R., Halpin, J.A., Baturina, E.L., Lyons, T.W., Wu, S., Danyushevsky, L., Sack, P.J., Chappaz, A., and Maslennikov, V.V., 2015, TE content of sedimentary pyrite in black shales: Economic Geology, v. 110, p. 1389–1410, https://doi.org/10.2113/econgeo.110.6.1389.
- Gregory, D.D., Lyons, T.W., Large, R.R., Jiang, G., Stepanov, A.S., Diamond, C.W., Figueroa, M.C., and Olin, P., 2017, Whole rock and discrete pyrite geochemistry as complementary tracers of ancient ocean chemistry: An example from the Neoproterozoic Doushantuo Formation, China: Geochimica et Cosmochimica Acta, v. 216, p. 201–220, https://doi.org/10.1016/j.gca.2017 .05.042.
- Gregory, D., Mukherjee, I., Olson, S.L., Large, R.R., Danyushevsky, L.V., Stepanov, A.S., Avila, J.N., Cliff, J., Ireland, T.R., and Raiswell, R., 2019, The formation mechanisms of sedimentary pyrite nodules determined by trace element and sulfur isotope microanalysis: Geochimica et Cosmochimica Acta, v. 259, p. 53–68, https://doi.org /10.1016/j.gca.2019.05.035.
- Gregory, D.D., Lyons, T.W., Large, R.R., and Stepanov, A., 2022, Ground-truthing the pyrite trace element proxy in modern euxinic settings: The American Mineralogist, https://doi.org/10.2138/am-2022-8024 (in press).
- Huerta-Diaz, M.A., and Morse, J.W., 1992, Pyritization of trace metals in anoxic marine sediments: Geochimica et Cosmochimica Acta, v. 56, p. 2681–2702, https://doi.org/10.1016/0016-7037(92)90353-K.
- Large, R.R., et al., 2009, Gold and trace element zonation in pyrite using a laser imaging technique:

- Implications for the timing of gold in orogenic and Carlin-style sediment-hosted deposits: Economic Geology, v. 104, p. 635–668, https://doi.org/10.2113/gsecongeo.104.5.635.
- Large, R.R., Halpin, J.A., Danyushevsky, L.V., Maslennikov, V.V., Bull, S.W., Long, J.A., Gregory, D.D., Lounejeva, E., Lyons, T.W., and Sack, P.J., 2014, TE content of sedimentary pyrite as a new proxy for deep-time ocean–atmosphere evolution: Earth and Planetary Science Letters, v. 389, p. 209–220, https://doi.org/10.1016/j.epsl.2013.12.020.
- Large, R.R., Mukherjee, I., Gregory, D., Steadman, J., Corkrey, R., and Danyushevsky, L.V., 2019, Atmosphere oxygen cycling through the Proterozoic and Phanerozoic: Mineralium Deposita, v. 54, p. 485–506, https://doi.org/10.1007/s00126-019-00873-9.
- Lowers, H.A., Breit, G.N., Foster, A.L., Whitney, J., Yount, J., Uddin, M.N., and Muneem, A.A., 2007, Arsenic incorporation into authigenic pyrite, Bengal Basin sediment, Bangladesh: Geochimica et Cosmochimica Acta, v. 71, p. 2699–2717, https:// doi.org/10.1016/j.gca.2007.03.022.
- Lyons, T.W., Werne, J.P., Hollander, D.J., and Murray, R.W., 2003, Contrasting sulfur geochemistry and Fe/Al and Mo/Al ratios across the last oxic-to-anoxic transition in the Cariaco Basin, Venezuela: Chemical Geology, v. 195, p. 131–157, https://doi.org/10.1016/S0009-2541(02)00392-3.
- Martin, J., Nirel, P., and Thomas, A., 1987, Sequential extraction techniques: Promises and problems: Marine Chemistry, v. 22, p. 313–341, https://doi.org/10.1016/0304-4203(87)90017-X.
- Ohfuji, H., and Rickard, D., 2005, Experimental syntheses of framboids—A review: Earth-Science Reviews, v. 71, p. 147–170, https://doi.org/10.1016/j.earscirev.2005.02.001.
- Owens, J.D., Reinhard, C.T., Rohrssen, M., Love, G.D., and Lyons, T.W., 2016, Empirical links between trace metal cycling and marine microbial ecology during a large perturbation to Earth's carbon cycle: Earth and Planetary Science Letters, v. 449, p. 407–417, https://doi.org/10.1016 /j.epsl.2016.05.046.
- Raven, M.R., Fike, D.A., Bradley, A.S., Gomes, M.L., Owens, J.D., and Webb, S.A., 2019, Paired organic matter and pyrite δ³⁴S records reveal mechanisms of carbon, sulfur, and iron cycle disruption during ocean anoxic event 2: Earth and Planetary Science Letters, v. 512, p. 27–38, https://doi.org /10.1016/j.epsl.2019.01.048.
- Rickard, D., 2012, Sulfidic Sediments and Sedimentary Rocks: Oxford, UK, Elsevier, 816 p.
- Rickard, D., 2019, How long does it take a pyrite framboid to form?: Earth and Planetary Science Letters, v. 513, p. 64–68, https://doi.org/10.1016/j.epsl.2019.02.019.
- Rickard, D., 2021, Framboids: New York, Oxford University Press, 360 p., https://doi.org/10.1093/oso/9780190080112.001.0001.
- Sack, P.J., Large, R.R., and Gregory, D.D., 2018, Geochemistry of shale and sedimentary pyrite as a proxy for gold fertility in the Selwyn Basin area, Yukon: Mineralium Deposita, v. 53, p. 997–1018, https://doi.org/10.1007/s00126-018-0793-5.
- Wacey, D., Kilburn, M.R., Saunders, M., Cliff, J.B., Kong, C., Liu, A.G., Matthews, J.J., and Brasier, M.D., 2015, Uncovering framboidal pyrite biogenicity using nano-scale CN_{org} mapping: Geology, v. 43, p. 27–30, https://doi.org/10.1130 /G36048.1.

Printed in USA